EXPERIMENTAL AND THEORETICAL ANALYSIS OF ANISOTROPIC MECHANICAL PROPERTIES OF ZIRCALOY FUEL ELEMENT CLADDINGS

G. DRESSLER, K.-H. MATUCHA, P. WINCIERZ

Metall-Laboratorium, Metallgesellschaft AG, D-6000 Frankfurt a. M., Germany

SUMMARY

As a result of the thermomechanical treatment during production Zircaloy canning tubes always show pronounced textures, which lead to anisotropic mechanical properties. On the basis of the knowledge of the multiaxial operational in-pile stresses and their tempora l changes the possibility of texture strengthening can be successfully used to optimize the performance of the fuel rods. The necessary supposition is a detailed experimental determination of the anisotropic mechanical properties in terms of the stress ratio α (α = axial stress: tangential stress) and the tube texture. Beyond that mathematical models which can be used for the core design and which take into account the material anisotropy have to be developed.

The elastic deformation and the onset of plastic flow of Zircaloy canning tubes under biaxial stress conditions were measured by applying simultaneously compressive or tensile stresses in the axial tube direction ($\pm\pi\delta_a$) and tangential stresses ($+\delta_t$). The apparent Young's moduli E_a and E_t, taken from the stress-strain diagrams, have different values and vary with the stress ratio α.

A similar stress and directional variation of the onset of flow was measured after passing the elastic region. The criteria valid for isotropic materials turned out to be not suited for a satisfactory description of the measured data and relations.

A calculation method covering the elastic deformation and the onset of yield as a result of biaxial stressing and considering tube textures was developed. The textures of Zircaloy tubes are characterized by a $\langle 10\bar{1}0 \rangle$ direction parallel to the tube axis. The (0002) basal poles are tilted by the angle $\pm\gamma$ towards the tangential tube direction in the plane given by the radial and tangential directions of the tube. For the given calculation the tube texture is substituted by two symmetrical single crystal orientations characterized by the tilt angles $+\gamma$ and $-\gamma$.

For the calculation of the *elastic* deformations the general Hooke's law is applied to the single crystal orientations. The calculation results in the reciprocal apparent Young's moduli $1/E_a'$ and $1/E_t'$ in terms of the elastic compliance constants S_{ij}, the stress ratio α and the tilt angle γ.

The *onset of plastic flow* is calculated as a continuation of the basic work of Hosford resp. Chin and Mammel. The general Schmid law is applied to the slip and mechanical twinning systems. It is taken into account that the twin systems can only be activated if the resultant shear deformation is compatible with the macroscopic deformation.

The calculation shows that the axial yield stress ($\alpha = \infty$) does not depend on the tilt angle γ of the basal poles, i.e. the texture. For other stress ratios the flow stress varies with γ, i.e. there is a marked texture dependence. The proposed calculation methods are discussed on the basis of the experimental results.

1. Introduction

Because of the directional variation of the plastic and elastic properties of Zircaloy cladding tubes the easy measurable axial data are not suited for the complete description of the mechanical behaviour of the material. The given possibility of texture hardening has in comparison with other strengthening mechanisms (i.e. solid solution or precipitation hardening) the advantage that the chemical composition of the material and with that the neutron absorption is kept constant.

In spite of the possibility to vary the texture in a broad range by a variation of the tube processing parameters the potential of texture strengthening is, according to our knowledge, not yet fully utilized because of the following reasons:

a) Texture strengthening has been quantitatively measured only for a few special textures,
b) the known calculation methods are not suited to predict the mechanical behaviour of Zircaloy tubes with different textures.

Therefore, the following work was undertaken with the aim of an experimental determination of the elastic and plastic anisotropy and the development of suitable calculation methods.

2. Experimental procedure

The experiments were performed using commercially produced Zircaloy-4 tubes (10.7 mm o. d. x 0.7 mm wall thickness). The chemical composition of the material was within the limits for Zircaloy-4 [1] with an oxygen content of 1140 - 1210 ppm. The tubes have been stress-relieved after the final cold deformation.

Material I corresponds to the standard Zircaloy-4 used as cladding material for water-cooled power reactors, whereas material II, being from the same ingot, was produced by an experimental production run, specially fabricated with regard to a difference in texture. The tube textures were determined by quantitative $\{0002\}$ and $\{01\bar{1}0\}$ pole figures using computerized techniques [2]. Fig. 1 shows the $\{0002\}$ pole figures for the two materials used. For brevity, we have not shown the $\{10\bar{1}0\}$ pole figures. The textures can be characterized by a $\langle 10\bar{1}0 \rangle$ direction parallel to the tube axis and the $\langle 0002 \rangle$ basal poles being tilted by variable angles $\pm\gamma$ towards the tangential tube direction in the plane given by the radial and tangential directions of the tube. The texture of material II (see Fig. 1b) can be described by two symmetrical single crystal orientations with $[01\bar{1}0]$ parallel to the tube axis and a tilt angle γ of the basal poles of $\pm 50^{\circ}$. Material I cannot be described by two single crystal orientations, but

by a number of single crystals having tilt angles γ in the range of $\pm 0^{o}$ to $\pm 30^{o}$.

The elastic deformations and the onset of plastic flow under defined, biaxial stresses were determined using an apparatus described earlier [3]. The tangential stresses ($+ \sigma_t$), created by internal pressurization of the tube samples, were superimposed by axial tensile or compressive stresses ($\pm \sigma_a$). The axial and tangential strains for constant stress rations ($\alpha = \sigma_a / \sigma_t$) were measured using strain ganges and conventional electronic equipment.

3. Results

3.1 Elastic properties

Fig. 2 shows characteristic stress-strain diagrams for the two types of tubing with different textures measured with a stress ratio of $\alpha = 1$. The slopes of the straight lines correspond to proportionality factors which are in the following defined as apparent Young's moduli E_a' and E_t'. The experimentally determined reciprocals of these moduli ($1/E_a'$ and $1/E_t'$) are plotted versus $1/\alpha$ or α in Fig. 3. $1/\alpha = 0$ ($\alpha = \infty$) corresponds to an uniaxial stress in the axial tube direction, $\alpha = 0$ to an uniaxial stress in the tangential direction.

From the experimental results given in Fig. 3a and 3b one can derive the following conclusions:

a) The measured values give straight lines for each material, showing a linear relationship between $1/E_a' = f\ (1/\alpha)$ and $1/E_t' = f\ (\alpha)$.
b) These two lines are nearly parallel.
c) $1/E_a'$ is identical for the two materials in the case of $1/\alpha = 0$, i.e. it does not depend on γ.
d) $1/E_t'$ is different for the two materials, i.e. it varies with γ.

3.2 Plastic properties

For the determination of the onset of plastic flow at constant α the values of σ_a und σ_t were measured which cause a plastic strain of 0.2 % in the axial or tangential tube direction. The resultant yield loci are given by Fig. 4a and b for material I resp. II. Fig. 4 additionally shows the tangents of the yield loci, calculated for specific points by

$$\frac{d\ \sigma_a}{d\ \sigma_t} = - \frac{d\ \varepsilon_a^{pl}}{d\ \varepsilon_t^{pl}} \qquad (1)$$

The yield loci clearly show the remarkable anisotropy of the

materials given by the deviation of the measured yield loci from the von Mises curves for isotropic material [4] and the different values for the 0.2 % yield stress in the axial and tangential tube directions (see Fig. 4b). Furthermore, for material II the 0.2 % yield stress in the range $0 \leq \alpha \leq 1$ only depends on the value of the tangential stress.

4. Calculation methods and comparison with experimental results

4.1 Elastic anisotropy

Calculation. The elasticity theory for isotropic materials cannot be used for an interpretation of the results given in Fig. 3 which shows different values for the Young's moduli for uniaxial stress conditions. Furthermore, this theory gives in the case of balanced biaxial tension ($\alpha = 1$) $E_a' = E_t'$. This proposition is not fulfilled as one can easily see from Fig. 2. These discrepancies lead to a modified calculation method using the following basic assumption: The texturized polycrystalline material is substituted by single crystals with orientations equal to the main volume fraction of the polycrystals. For example, material II is substituted by two single crystals with the $[01\bar{1}0]$ direction parallel to the tube axis and tilt angles γ of $\pm 50^{\circ}$ corresponding to the maximum intensity seen from Fig. 1b.

The general Hooke's law [5] is applied to these single crystals. The stresses σ_{ij} and the strains ε_{ij} are related by the compliance constants S_{ij} of the single crystals. ε_{ij} and σ_{ij} can be described by an orthogonal coordinate system which is adapted to the hexagonal crystal structure. The coordinate axes are given by the $[2\bar{1}\bar{1}0]$, $[01\bar{1}0]$ and $[0002]$ crystal directions (comp. Fig. 5). The calculation comprises four steps:

a) The components of the stress tensor σ_{ij} are expressed by σ_a, σ_t and γ :

$$\sigma_{ij} = l_{it}\, l_{jt}\, \sigma_t + l_{ia}\, l_{ja}\, \sigma_a \qquad (2)$$

l_{it} is the direction cosine between the direction i and the tangential direction; l_{jt}, l_{ia} and l_{ja} are defined in an analogue manner.

b) From the general Hooke's law the strains ε_{ij} are calculated as functions of S_{ij}, σ_a, σ_t and γ.

c) The axial and tangential strains ε_a and ε_t are calculated from the ε_{ij} values.

d) Using $\alpha = \sigma_a / \sigma_t$ one finally can derive stress-strain equations.

These calculations (see Appendix) result in the equations:

$$\frac{1}{E_a'} = m_a \cdot \frac{1}{\alpha} + b_a \qquad (3)$$

$$\frac{1}{E_t'} = m_t \cdot \alpha + b_t \qquad (4)$$

The constants are given by:

$$b_a = S_{11} \qquad (5)$$

$$m_a = m_t = S_{12}\cos^2\gamma + S_{13}\sin^2\gamma \qquad (6)$$

$$b_t = S_{11}.\cos^4\gamma + S_{33}.\sin^4\gamma + (S_{44} + 2S_{13})\ \sin^2\gamma\cos^2\gamma \qquad (7)$$

Eq. (3) and (4) give the relations between the axial and tangential Young's moduli and the crystal orientation (expressed by γ) in the case of a biaxial stress system.

With $\alpha = 0$ resp. $1/\alpha = 0$ one obtains from eqs. (3) and (4) the well known equations for the special case of an uniaxial stress system [5].

Comparison with experimental results. For a given texture, i.e. γ = const., a diagram as plotted in Fig. 3 has to result in straight lines following eqs. (3) and (4). These lines should be parallel, see eq. (6). For different textures, i.e. materials I and II, the intercept on the $1/E_a'$-axis have to coincide ((eqs. (3) and (5)) and correspond to S_{11} (eq. (5)). These two theoretic predictions are consistent with the experimental data (Fig. 3). Beside these qualitive results the following quantitative conclusions can be drawn:

S_{11} has a value of $10 \pm 0{,}3 \times 10^{-5}$ mm^2/kg, which is in good agreement with the published single crystal value [6] of 10.1×10^{-5} mm^2/kg for pure α-Zirconium. The other compliance constants [6] were used to calculate the straight lines given in Fig. 3b with $\gamma = 50^\circ$ and eqs. (3) and (4). This also results in a good quantitative agreement with the experimental results.

Taken into account the more scattered texture of material I (Fig. 1a) calculations were made for $\gamma = 0^\circ$ and $\gamma = 30^\circ$. According to Fig. 3a the measured data are in the range of the calculated values.

4.2 Plastic anisotropy

Calculation. For the mathemathical treatment of the plastic deformations the General Schmid law is applied. The acting stress σ_{eg} is calculated for each crystallographic deformation system.which is defined by a crystallographic plane e and a direction g.

Plastic flow starts if the stress σ_{eg} reaches a critical value τ_o. The calculation leads to a flow condition for each deformation system n:

$$\tau_{on} = a_n \sigma_a + b_n \cdot \sigma_t \qquad (8)$$

a_n and b_n can be calculated from the orientation relationship between the deformation system n and the coordinate system given by the acting stresses.

The lack of data on the critical resolved shear stresses (CRSS) for single crystals can be overcome by normalizing all stresses to the CRSS(= τ_o). The graph $\sigma_a / \tau_o = f(\sigma_t / \tau_o)$ gives straight lines for each specific deformation system (yield lines). The whole yield lines can be composed from the yield lines of the different deformation systems. This is shown in Fig. 6 for a copper single crystal. This calculation method has up to now only been applied for hexagonal metals to slip systems [7] but not to the twinning systems which play an important role during the plastic deformation of zirconium.

For this reason, the calculation method for prismatic slip is transferred to twinning deformation. In addition to this mathematical treatment it has to be considered that twinning systems will only be activated if the resulting shear deformation is compatible with the overall macroscopic deformation. Due to the fact that the active twinning systems either cause shortening ($\{11\bar{2}2\}\langle 11\bar{2}\bar{3}\rangle$ system*)) or elongation ($\{10\bar{1}2\}\langle 10\bar{1}\bar{1}\rangle$ resp. $\{11\bar{2}1\}\langle 11\bar{2}\bar{6}\rangle$ systems) in the direction of the c-axis [8], the active twin systems can be selected as follows: Before the plastic flow starts the deformation directions of the crystals can be predicted by the elastic properties in conjunction with the macroscopic stresses. It is assumed that this deformation directions will not discontinuously change when the yield point is passed.

For example, for a tilt angle of $\gamma = 0^o$ (i.e. the c-axis is parallel to the radial tube direction) in the tension-tension quadrant I of the yield locus the c-axis will first be elastically shortened and a $\{11\bar{2}2\}\langle 11\bar{2}\bar{3}\rangle$ -twinning system can be activated if the CRSS of this system is reached. In the compression-compression quadrant IV of the yield locus, however, the other two twin systems become active.

It can generally be shown that a stress ratio α_c exists for each tilt angle γ which results in a strain free c-axis (compare with Appendix):

$$\alpha_c(\gamma) = \left(1 - \frac{S_{33}}{S_{13}}\right) \sin^2\gamma - 1 \qquad (9)$$

---

*) A twinning system is characterized by the crystallographic twinning plane {hkil} and the twinning shear direction ⟨uvtw⟩ in the twinning plane.

If $\alpha > \alpha_c(\gamma)$ the c-axis will be elastically shortened and for all $\alpha < \alpha_c(\gamma)$ there will be an elastic elongation of the c-axis. The function $\alpha_c(\gamma)$ therefore divides the $\sigma_a - \sigma_t$-plane into two regions with different active twinning systems.

Additionally, in contrast to the known calculation of yield loci for fcc metals [9], for zirconium one has to consider that prismatic slip or the different twinning systems have different critical resolved shear stresses. Therefore a normalization of calculated yield loci is problematic. This difficulty can be solved by expressing the CRSS for twinning τ_i as a function of the CRSS for prismatic slip (τ_p):

$$\tau_i = k_i \cdot \tau_p \qquad (10)$$

i = number of twinning systems

k_i is a specific constant for each twinning system. Therefore, one obtains for prismatic slip from eq. (8)

$$\frac{\sigma_a}{\tau_p} = -\frac{b_p}{a_p}\,\frac{\sigma_t}{\tau_p} + \frac{1}{a_p} \qquad (11)$$

and respectively for the twinning system i

$$\frac{\sigma_a}{\tau_i} = -\frac{b_i}{a_i}\,\frac{\sigma_t}{\tau_i} + \frac{1}{a_i} \qquad (12)$$

Eqs. (10) and (12) give:

$$\frac{\sigma_a}{\tau_p} = -\frac{b_i}{a_i} \cdot \frac{\sigma_t}{\tau_p} + \frac{k_i}{a_i} \qquad (13)$$

Eq. (13) means that the slope of the yield line, $\frac{b_i}{a_i}$ is independent on $k_i = \frac{\tau_i}{\tau_p}$, while the intercepts on the σ_a-axis depend on the k_i-values.

Fig. 7 shows calculated yield loci for three different single crystal orientations ($\gamma = 0$; $\gamma = \pm 30^\circ$; $\gamma = \pm 50^\circ$). With regard to the relationship between the shape of the yield loci and the tilt angle the following conclusions can be made (see Fig. 7):

a) The points of intersection of the yield lines with the σ_a-axis do not depend on γ.

b) The slopes of the yield lines having a finite intersection point with the σ_a-axis depend on γ. The slope is proportional to $\cos^2\gamma$ in case of prismatic slip and to $\sin^2\gamma$ for $\{10\bar{1}2\}$-twinning.

c) The points of intersection of the yield lines with the σ_t-axis vary with γ.

d) The critical stress ratio α_c causing a strain-free c-axis increases with increasing tilt angle γ (Eq. (9)).

Comparison with experimental results. Due to the fact that the yield loci were calculated for single crystals especially material II is suited for an experimental revision of the calculated data. From Fig. 7 it can be seen that the calculated yield locus for $\gamma = 50^\circ$ has a similar shape as the measured locus (Fig. 4b). Using the ratios of 1 : 1.25 : 1.35 : 1.4 for the constants k_i (Eq. (10)) one obtains the calculated locus given in Fig. 4b. For the more diffuse texture of material I we have calculated the whole set of yield loci for single crystals with $\gamma = 0 - 30^\circ$. The plotted locus (Fig. 4a) has been selected from those yield lines which contribute first to a plastic deformation at any given stress ratio.

Regarding Figs. 4a and 4b it generally can be said that the calculated loci are in a fairly good agreement with the measured ones. The existing differences can mainly be traced back to the fact that the real textures have been substituted by special single crystal orientations, only regarding for instance crystals with c-axis in the plane given by the radial and tangential tube directions.

5. Conclusions

1) The proposed calculation method for the elastic anisotropy is suited to predict the elastic properties for textured Zircaloy in the case of biaxial stress systems.

   The compliance constants determined for pure zirconium single crystals are, according to the described agreements between calculated and experimental data, also appliable for Zircaloy.

2) Although the proposed model for the calculation of plastic anisotropy (yield loci) is only applied on the basis of a simplified description of the material texture, a sufficient agreement with the experimental results is reached. We consider the proposed methods being the first step towards a more detailed and accurate mathematical treatment which takes into account the volume fraction of all really observed crystal orientations.

Appendix: 1.) Deduction of eqs. (3) and (4)

Step a (see pp. 4): The direction cosine for the considered single crystal orientations are given by (see Fig. 5):

$$l_{1t} = \cos\gamma; \quad l_{1a} = l_{2t} = l_{3a} = 0; \quad l_{2a} = 1; \quad l_{3t} = \sin\gamma$$

Therefore eq. (2) gives:

$$\left.\begin{array}{l} \sigma_{11} = \cos^2\gamma\ \sigma_t; \quad \sigma_{12} = \sigma_{23} = 0; \ \sigma_{13} = \cos\gamma \sin\gamma\ \sigma_t \\ \sigma_{33} = \sin^2\gamma\ \sigma_t; \quad \sigma_{22} = \sigma_a \end{array}\right\} \qquad (14)$$

Step b: Replacing σ_{ij} by eqs. (14) in the General Hooke's law [5] results in:

$$\varepsilon_{11} = S_{11} \cos^2\gamma\ \sigma_t + S_{12}\,\sigma_a + S_{13} \sin^2\gamma\ \sigma_t$$

and analogue equations for the other ε_{ij}.

Step c: ε_a and ε_t are calculated by:

$$\varepsilon_a = \sum_{i,j=1}^{3} l_{ia} l_{ja}\, \varepsilon_{ij} \qquad (15) \quad \text{resp. } \varepsilon_t = \sum_{i,j=1}^{3} l_{it} l_{jt}\, \varepsilon_{ij} \qquad (16)$$

Step d: With $\sigma_t = \frac{1}{\alpha}\ \sigma_a$ resp. $\sigma_a = \alpha . \sigma_t$ one obtains from eqs. (15) resp. (16) the final eqs. (3) and (4) given in the text.

2. Deduction of eq. (9)

From step b one obtains:

$$\varepsilon_{33} = S_{13} \cos^2\gamma\ \sigma_t + S_{13}\ \sigma_a + S_{33} \sin^2\gamma\ \sigma_t.$$

With $\varepsilon_{33} = 0$ and $\alpha = \frac{\sigma_a}{\sigma_t}$ eq. (9) results.

References:

[1] ASTM B353-64T, Grade RA-2

[2] GREWEN, J., SAUER, D., WAHL, H.-P., "Automatisierte quantitative Texturbestimmung an Blechen ohne regellose Vergleichsprobe", Z. Metallkde. 61, 430 (1970)

[3] DRESSLER, G., MATUCHA, K.-H., WINCIERZ, P., "Yield loci of Zircaloy tubing with different textures", Can. Met. Quarterly 11, 177 (1972)

[4] VON MISES, R., Z. angew. Math. Mech. 8, 161, (1928)

[5] NYE, J. F., "Physical Properties of Crystals", Claredon, Oxford 1957, pp. 141 - 144

[6] FISHER, E. S., RENKEN, G. J., "Adiabatic elastic moduli of single crystal alpha zirconium", J. nucl. Mat. 4, 311 (1961)

[7] CHIN, G. Y., MAMMEL, W. L., "Competition among basal, prism, and pyramidal slip modes in hcp metals", Met. Trans. 1, 357 (1970)

[8] DOUGLASS, D. L., "The Metallurgy of Zirconium", Atomic Energy Review, Suppl. 1971, pp. 42, IAEA Vienna, 1971

[9] PIEHLER, H. R., BACKOFEN, W. A., "The Prediction of Anisotropic Yield for Textured Sheets" in: Grewen, J., Wassermann, G. (Eds.), "Texturen in Forschung und Praxis", Springer, Berlin 1969, pp. 436-443.

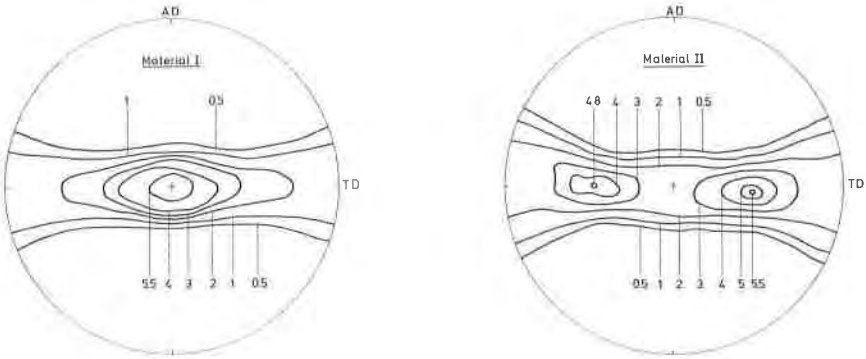

Fig. 1a, b: Quantitative {0002} pole figures

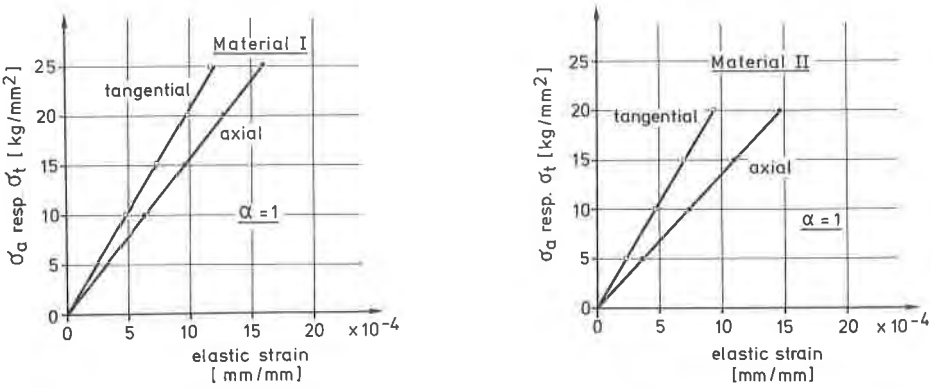

Fig. 2a, b: Stress-strain-diagrams

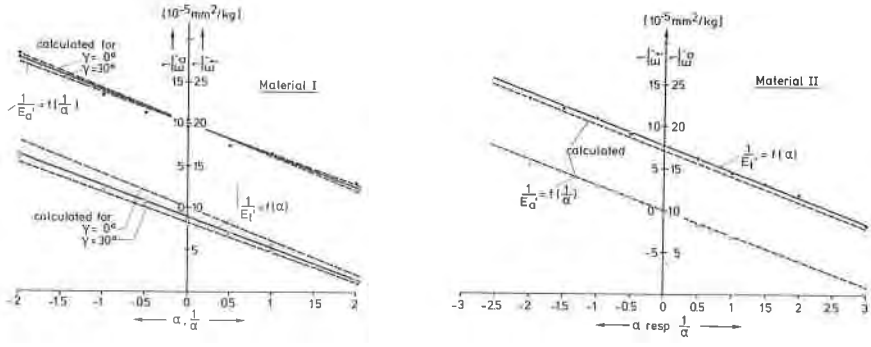

Fig. 3a, b: Variation of reciprocal apparent Young's moduli with stress ratio

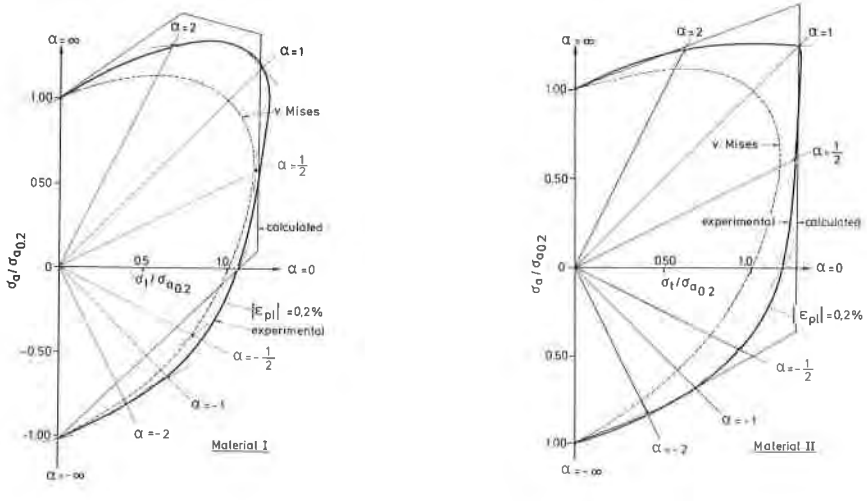

Fig. 4a, b: Yield loci for Zircaloy-4 tubing

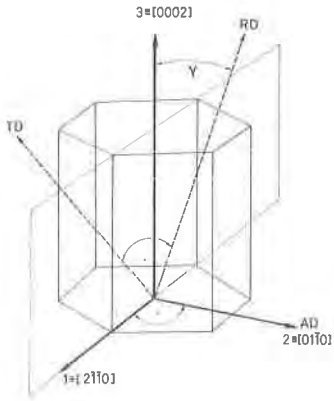

Fig. 5: Schematic representation of used coordinate systems

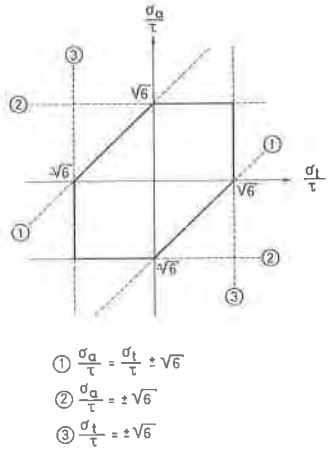

Fig. 6: Calculated yield locus for a copper single crystal with [100] ∥ σ_t and [010] ∥ σ_a. The complete yield locus is constructed from the yield lines ①, ②, ③.

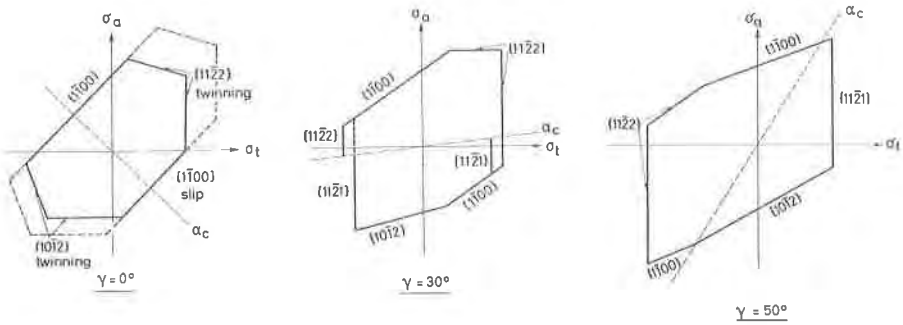

Fig. 7a-c: Calculated yield loci. Ratio of CRSS for {1$\bar{1}$00} -slip, {10$\bar{1}$2}-, {11$\bar{2}$1}-, and {11$\bar{2}$2}-twinning = 1 : 1 : 1 : 1 resp. = 1 : 1.25 : 1.35 : 1.4 (dashed lines in Fig. 7a).